Wideband Measurements of the Forward RCS and the Extinction Cross Section

Larsson, Christer; Gustafsson, Mats

Published in:
[Host publication title missing]

2012

WIDEBAND MEASUREMENTS OF THE FORWARD RCS AND THE EXTINCTION CROSS SECTION

Christer Larsson*† and Mats Gustafsson†

*Saab Dynamics
S-581 88 Linköping
Sweden

†Department of Electrical and Information Technology
Lund University
P.O. Box 118
S-221 00 Lund
Sweden

ABSTRACT

This paper describes the development of a method based on measurements of the radar cross section (RCS) in the forward direction to determine the extinction cross section for the 2.5–38 GHz frequency range using the optical theorem. Forward RCS measurements are technically complicated due to that the direct signal has to be subtracted from the total signal at the receiving antenna in order to extract the forward RCS. The efficiency of this subtraction as a function of time is evaluated. A traditional calibration method using a calibration target and a second method that does not require a calibration target are investigated and compared. The accuracy of the forward RCS measurements is determined using small spheres of different sizes. The spheres have a forward RCS that is straightforward to calculate with good accuracy. The method is also extended to polarimetric measurements on a small helix that are compared to theoretical calculations.

Keywords: Bistatic, Calibration, Extinction Cross Section, Forward RCS, Measurement, Polarimetry

1 Introduction

This study treats the development of a method to determine the extinction cross section for the 2.5–38 GHz frequency range. The method is based on measurements of the radar cross section (RCS) in the forward direction in a conventional anechoic chamber designed for monostatic measurements. The extinction cross section is then calculated from the measured forward RCS using the optical theorem.

The motivation for this work is to develop an experimental method that can be used to verify theoretical work which shows that the extinction cross section integrated over all frequencies is related to the static properties of the scatterer [1, 2].

Forward RCS measurements are technically complicated due to the large direct contribution from the transmitting antenna to the received signal. The direct signal has to be subtracted from the total signal at the receiving antenna in order to extract the forward RCS. The efficiency of this subtraction is evaluated in this study by performing long time measurements leading to an estimation of subtraction accuracy as a function of the time between the two measurements.

Two calibration methods are investigated. The first method is the traditional calibration method used in most RCS measurements. It uses a target with known RCS as a calibration target to calibrate the target measurement. The second method that is described here uses only a direct path measurement of the signal to calibrate the target measurement without any calibration object. To the best of our knowledge, the latter method is not in frequent use in the RCS community.

The method described here is also extended to polarimetric measurements of the forward RCS and hence the possibility to determine the extinction cross section for arbitrarily polarized incident radiation. This is tested using measurements on a small helix coil and comparing with method of moments calculations. More details of the experimental methods can be found in [3].

2 Theory

Consider the direct scattering problem of a time harmonic plane electromagnetic wave impinging in the $\hat{\boldsymbol{k}}$-direction on a bounded scatterer. The bistatic RCS, $\sigma(f, \hat{\boldsymbol{r}})$, in the $\hat{\boldsymbol{r}}$ di-

rection at the frequency f is then defined as [4],

$$\sigma(f,\hat{\boldsymbol{r}}) = \lim_{r\to\infty} 4\pi r^2 \frac{|\boldsymbol{E}_\mathrm{s}(\boldsymbol{r})|^2}{|\boldsymbol{E}_\mathrm{i}|^2}, \tag{1}$$

where $\boldsymbol{E}_\mathrm{i}$ denotes the incident electric field, $\boldsymbol{E}_\mathrm{s}$ denotes the scattered electric field and $r = |\boldsymbol{r}|$ denotes the magnitude of the position vector $\boldsymbol{r} = r\hat{\boldsymbol{r}}$. Introduce the complex-valued bistatic RCS amplitude, $\boldsymbol{A}(f,\hat{\boldsymbol{r}})$, in the $\hat{\boldsymbol{r}}$ direction. $\boldsymbol{A}(f,\hat{\boldsymbol{r}})$ preserves the phase information in the measurement and it is defined as,

$$\boldsymbol{A}(f,\hat{\boldsymbol{r}}) = \lim_{r\to\infty} 2\sqrt{\pi} r \frac{\boldsymbol{E}_\mathrm{s}(\boldsymbol{r})}{|\boldsymbol{E}_\mathrm{i}|} \mathrm{e}^{-\mathrm{i}kr}, \tag{2}$$

where it is assumed that the time convention is $\mathrm{e}^{-\mathrm{i}\omega t}$ for the time harmonic wave and $k = 2\pi f/\mathrm{c}_0$. c_0 is the phase velocity of light in free space.
$\sigma(f,\hat{\boldsymbol{r}})$ and $\boldsymbol{A}(f,\hat{\boldsymbol{r}})$ are then related by,

$$\sigma(f,\hat{\boldsymbol{r}}) = |\boldsymbol{A}(f,\hat{\boldsymbol{r}})|^2. \tag{3}$$

In practice, the two polarization components of $\boldsymbol{A}(f,\hat{\boldsymbol{r}})$ are measured separately for an incident wave that is transmitted with a defined polarization. This means that measured RCS data usually is presented as a function of the transmitted and received polarizations, *e.g.*, σ_VH and A_VH are the notations for the recorded RCS and RCS amplitude component, respectively, for vertical transmitting and horizontal receiving linear polarizations.
The scattering cross section, $\sigma_\mathrm{s}(f)$, is the average of the bistatic RCS over all angles,

$$\sigma_\mathrm{s}(f) = \frac{1}{4\pi}\int_\Omega \sigma(f,\hat{\boldsymbol{r}})\,\mathrm{d}\Omega, \tag{4}$$

where Ω and $\mathrm{d}\Omega$ denote the unit sphere and the surface element of the unit sphere, respectively. The extinction cross section, $\sigma_\mathrm{ext}(f)$, also designated the total cross section [5], is defined as

$$\sigma_\mathrm{ext}(f) = \sigma_\mathrm{s}(f) + \sigma_\mathrm{a}(f), \tag{5}$$

where $\sigma_\mathrm{a}(f)$ is the absorption cross section. The extinction cross section can be determined using (5) by measuring the bistatic RCS at all angles and the absorption cross section. However, a more straightforward method is to measure the RCS amplitude in the forward direction, $\boldsymbol{A}(f,\hat{\boldsymbol{k}})$, and use the optical theorem to determine $\sigma_\mathrm{ext}(f)$ [6].

$$\sigma_\mathrm{ext}(f) = \frac{\mathrm{c}_0}{\sqrt{\pi} f}\,\mathrm{Im}\,A_\mathrm{ii}(f,\hat{\boldsymbol{k}}), \tag{6}$$

where $A_\mathrm{ii}(f,\hat{\boldsymbol{k}})$ is the component of $\boldsymbol{A}(f,\hat{\boldsymbol{k}})$ that is co-polarized with the incident electric field, $\boldsymbol{E}_\mathrm{i}$, *i.e.*,

$$A_\mathrm{ii}(f,\hat{\boldsymbol{k}}) = \boldsymbol{A}(f,\hat{\boldsymbol{k}}) \cdot \frac{\boldsymbol{E}_\mathrm{i}^*}{|\boldsymbol{E}_\mathrm{i}|} \tag{7}$$

3 Measurements

Forward RCS measurements are performed in an anechoic chamber originally designed for monostatic RCS measurements. A pair of wideband ridged horn antennas are positioned facing each other at a distance of 6.80 m with the sample placed on an expanded polystyrene (EPS) column at the midpoint, see Fig. 1. The measurement uses a Performance Network Analyzer (PNA) transmitting a continuous wave without online hard or software gating. The source power from the PNA is set to 1 mW for the measurements described here. The power output from the antenna is significantly lower mainly due to cable losses. Two separate measurements using different antennas are performed for each sample in the frequency intervals 1–22 GHz and 16–40 GHz. Each interval is swept using 4000 frequency points. Eight such sweeps are averaged for each of the sample measurement, background measurement and calibration measurement.
Calibration measurements are performed using the two methods described in section 4.1.
The sample is measured and the direct path data is subtracted from the sample data. The processed sample data is then calibrated with the calibration vectors obtained using the two calibration methods. The calibrated data is finally gated with a 3.3 ns window in the time domain, chosen to aquire the entire target response and to minimize the influence of the background. The time domain filtering, as well as a large antenna beam width at low frequencies, reduces the useful frequency range to 2.5–38 GHz.

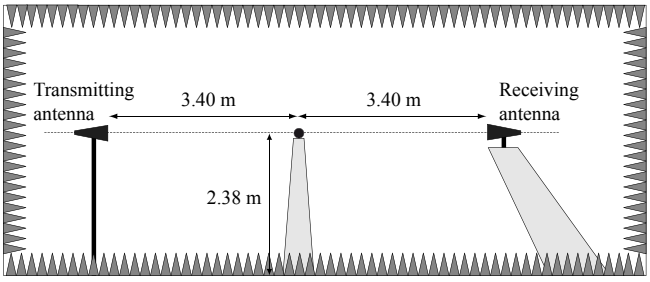

Figure 1. The figure shows the experimental setup in the anechoic chamber.

4 Results and discussion

4.1 Calibration

The first calibration method described here using a calibration target is the standard method for RCS calibration [4]. The RCS amplitude is determined from the difference between a measurement with the scattering target present and a measurement without target. The RCS amplitude component $A_\mathrm{ij}(f)$ defined previously with i and j transmitted and received polarizations, respectively, is then given by

$$A_\mathrm{ij}(f) = v_\mathrm{ij}(f)(V_\mathrm{ij,r}(f) - V_\mathrm{ij,d}(f)), \tag{8}$$

where $v_{\mathrm{ij}}(f)$ is the complex-valued calibration vector for the setup, $V_{\mathrm{ij,r}}(f)$ is the complex-valued amplitude as measured at the receiver with a scattering target, and $V_{\mathrm{ij,d}}(f)$ is the complex-valued amplitude as measured at the receiver without a scattering target.

In this method $v_{\mathrm{ij}}(f)$ is determined in a calibration measurement using a target with known RCS amplitude, $A_{\mathrm{ij,cal}}(f)$.

$$v_{\mathrm{ij}}(f) = \frac{A_{\mathrm{ij,cal}}(f)}{(V_{\mathrm{ij,r,cal}}(f) - V_{\mathrm{ij,d}}(f))}, \tag{9}$$

where $V_{\mathrm{ij,r,cal}}(f)$ is the measured amplitude at the receiver for the calibration target.

Spheres are ideal forward RCS calibration objects for several reasons. The RCS is easy to calculate to very good accuracy using the Mie series, see Ref. [5]. The symmetry of a sphere means that it is straightforward to align. A sphere has also a much larger forward RCS than its monostatic RCS. In fact, a sphere's forward RCS is similar to the forward RCS of a flat plate with the same cross section area.

It is also of interest to find a method that does not require a calibration target. This alternative method is based on measuring the direct signal from transmitting to receiving antenna and using it to calibrate [8].

The transmitting and receiving antennas are positioned facing each other at distance r_{d} between the antenna phase centers so that the direct path signal can be measured. Assuming that the transmitting antenna generates a spherical wave, the measured amplitude component at the receiving antenna for an empty setup can be written

$$V_{\mathrm{ij,d}}(f) = \frac{F_0 \mathrm{e}^{\mathrm{i}kr_{\mathrm{d}}}}{2\sqrt{\pi} r_{\mathrm{d}}}, \tag{10}$$

where F_0 is the far field of the transmitting antenna and r_{d} is the distance between the antenna phase centers. The incident field at the object position r_{t} is

$$E_0 = \frac{F_0 \mathrm{e}^{\mathrm{i}kr_{\mathrm{t}}}}{2\sqrt{\pi} r_{\mathrm{t}}}, \tag{11}$$

and the far field amplitude of the scattered field is $F = SE_0$, where S is the scattering coefficient. The received signal with object present is

$$V_{\mathrm{ij,r}}(f) = V_{\mathrm{ij,d}}(f) + \frac{SE_0 \mathrm{e}^{\mathrm{i}kr_{\mathrm{r}}}}{2\sqrt{\pi} r_{\mathrm{r}}} = V_{\mathrm{ij,d}}(f) + \frac{SF_0 \mathrm{e}^{\mathrm{i}kr_{\mathrm{d}}}}{4\pi r_{\mathrm{t}} r_{\mathrm{r}}}, \tag{12}$$

were r_{r} is the distance between the target and the receiving antenna, $r_{\mathrm{r}} + r_{\mathrm{t}} = r_{\mathrm{d}}$. We can then solve for the scattering coefficient as

$$S = \frac{V_{\mathrm{ij,r}}(f) - V_{\mathrm{ij,d}}(f)}{V_{\mathrm{ij,d}}(f)} \frac{2\sqrt{\pi} r_{\mathrm{t}} r_{\mathrm{r}}}{r_{\mathrm{d}}} \tag{13}$$

This expression is equal to the complex valued RCS amplitude for the object, $A_{\mathrm{ij}}(f)$, and can be used to calculate the RCS by (3) and the extinction cross section by (6). The calibration vector, $v_{\mathrm{ij}}(f)$, can be identified as

$$v_{\mathrm{ij}}(f) = \frac{2\sqrt{\pi} r_{\mathrm{t}} r_{\mathrm{r}}}{r_{\mathrm{d}} V_{\mathrm{ij,d}}(f)}. \tag{14}$$

A comparison between the two methods is made by performing forward RCS measurements on small metal spheres, with different radii a and calibrating the measured data with both calibration methods. The results of these measurements are shown in Fig. 2. The first calibration method using a calibration target gives a more accurate result than the second method. In fact, the data calibrated in this way is so close to the theoretical results that the curve is hard to distinguish from the theoretical curve in the figure. A calibration with the second calibration method using the direct path measurement to obtain a calibration vector results in a forward RCS that deviates up to 0.7 dB from the Mie result. It is not clear what causes the discrepancies for the second calibration method. Further studies are needed in order to investigate this.

The equation (6) is used to determine the extinction cross section for horizontally polarized incident electric field from the forward RCS amplitude, shown in Fig. 2, with similar results.

4.2 Background Subtraction

Consecutive background measurements of the forward scattering amplitude, $A_{\mathrm{bg}}(f, \hat{\boldsymbol{k}})$, are performed to determine the efficiency of the background subtraction as a function of time. $A_{\mathrm{bg,0}}(f, \hat{\boldsymbol{k}})$ is the forward scattering amplitude measured at $t = t_0$ and $A_{\mathrm{bg,n}}(f, \hat{\boldsymbol{k}})$ is the forward scattering amplitude measured at $t = t_n$ with $t_n > t_0$. The subtraction efficiency is defined according to Eq. 15. Here $\eta(f_0, t_{\mathrm{n}})$ is the subtraction efficiency for the frequency $f = f_0$ at time $t = t_n$. The efficiency is obtained by averaging over a frequency interval centered at $f = f_0$ with k frequency points,

$$\eta(f_0, t_{\mathrm{n}}) = \frac{1}{k} \sum_{\mathrm{i}} \left| \frac{A_{\mathrm{bg,n}}(f_{\mathrm{i}}, \hat{\boldsymbol{k}}) - A_{\mathrm{bg,0}}(f_{\mathrm{i}}, \hat{\boldsymbol{k}})}{A_{\mathrm{bg,n}}(f_{\mathrm{i}}, \hat{\boldsymbol{k}})} \right|^2 \tag{15}$$

Fig. 3 shows the subtraction efficiency, η, as a function of time for six different, 2 GHz wide, frequency bands. The bands with 6, 12 and 18 GHz center frequencies are measured at the same time and the bands with 24, 30 and 36 GHz center frequencies are measured at the same time but on another day. As expected and seen in the figure, the subtraction is most efficient at low frequencies. With reduced wavelength the effect of displacements becomes larger. The losses also increase with increased frequency which means a reduced signal to noise ratio (SNR). The reduced SNR also reduces the efficiency of the subtraction. The figure shows that the background subtraction is most efficient if the subtraction is performed within a few minutes relative to t_0. Focusing on

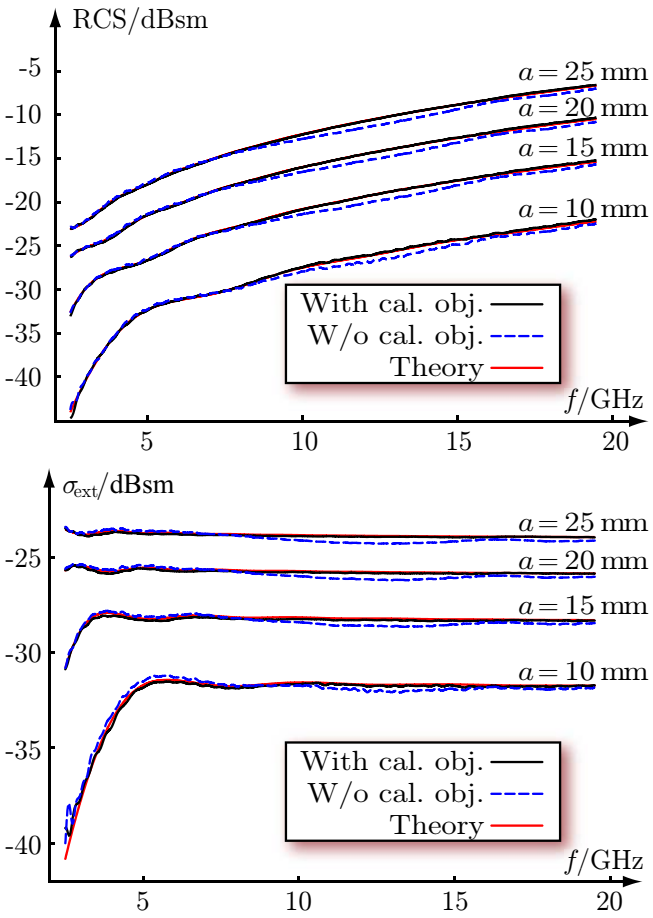

Figure 2. Comparison between results from forward RCS measurements on metal spheres using the two calibration methods described (top figure). The corresponding results for the extinction cross section are shown in the bottom figure. The results obtained from a Mie series calculation are shown as a reference.

the first 4 h of the measurements it is seen that the curves are not monotonically increasing. Instead, the subtraction is more efficient at $t = 4$ h than at $t = 2$ h.

This is interpreted as due to a change in distance between transmitting and receiving antenna. This interpretation is confirmed by a corresponding phase shift in the background measurement data. It is likely that this change in distance is caused by small chamber contractions or expansions due to temperature changes. Estimates of the temperature changes that are required to obtain these results can be made assuming a 6.8 m antenna to antenna distance, a chamber steel support structure and a coefficient of linear expansion of $11.7 \cdot 10^{-6}/^{\circ}\mathrm{C}$ for steel [9]. The subtraction efficiency is –63 dB for the 6 GHz curve at $t = 2$ h and –30 dB for the 36 GHz curve at $t = 3$ h. Assuming that the background subtraction efficiency is limited by relative displacements of the antennas, displacements of 5.6 μm and 24 μm are calculated for 6 GHz and 36 GHz, respectively. Using the antenna to antenna distance and the coefficient for linear expansion for steel, the error levels correspond to temperature changes of 0.07 °C and 0.3 °C, respectively. This means that it is extremely important to maintain a stable temperature if a good background subtraction efficiency is desired.

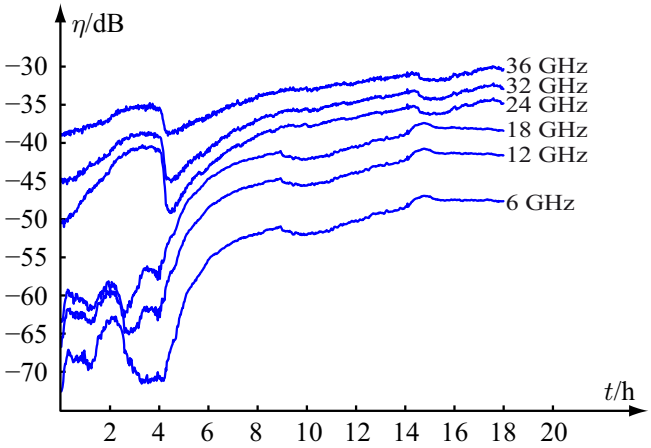

Figure 3. The figure shows the subtraction efficiency as a function of time, in hours, for $\Delta f = 2$ GHz wide frequency bands. The curves are labeled with the center frequencies of the frequency bands.

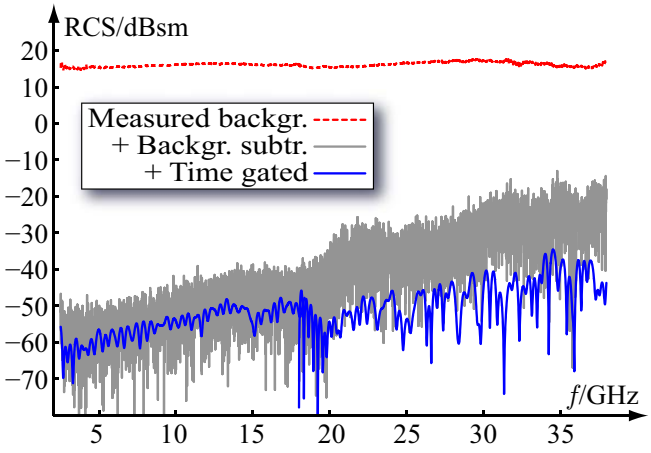

Figure 4. Measurement of the background. The figure shows calibrated raw data from a background measurement, data after subtracting another background measurement, and after additional time gating.

The result of a forward RCS measurement of the empty chamber is shown in Fig. 3. The figure also shows the results after coherent background subtraction and time domain gating. The performed background subtraction suppresses

the background by more than 70 dB which gives a background level of less than –55 dBsm at the lower frequencies. The background suppression becomes gradually less efficient with increasing frequency and gives a background of less than –25 dBsm at the highest frequencies. Time domain gating reduces the background by another 5 dB for the lower frequencies and 20 dB for the higher frequencies, see Fig. 4.

4.3 Polarimetric measurements

The cross-polarization distortion in the transmit and receive channels can be estimated measuring the background signal using the setup in Figure 1 without a target. Figure 5 shows the results from such a measurement of the calibrated background signal for the HH and HV components. The suppression, *i.e.*, the difference between the two curves, varies from approximately 20 dB to more than 30 dB depending on frequency.

The forward RCS of a helix,is measured with the incident wave direction, $\hat{\boldsymbol{k}}$, along the axis of the helix. A helix is chosen because it is expected to give different extinction cross sections for different circular polarizations of the incident wave. The four linearly polarized components, HH, VV, HV and VH, of the forward RCS obtained from a measurement of the helix sample are shown in Figure 6. The corresponding forward components of the RCS amplitude are used to determine the circular polarized components.

The corresponding forward RCS amplitude components can be used with (6) to obtain extinction cross sections for circular polarized incident waves. The resulting extinction cross sections for the helix for left circular polarized incident wave and for a right circular polarized incident wave are shown in Figure 7. There is also, as expected, a large difference between the two polarizations due to the geometry of the helix. The results are compared with method-of-moments calculations to validate the method. It is found that the measured and calculated results qualitatively agree well.

Polarimetric calibration to reduce the effect of cross-polarization distortion in the transmit and receive channels is considered for future development of the method presented in this paper. One could *e.g.*, use methods analogous to polarimetric calibration methods suggested for monostatic measurements, see *e.g.*, [10]. However, finding a calibration object for broadband forward scattering polarimetric calibration is more complicated than in the monostatic case.

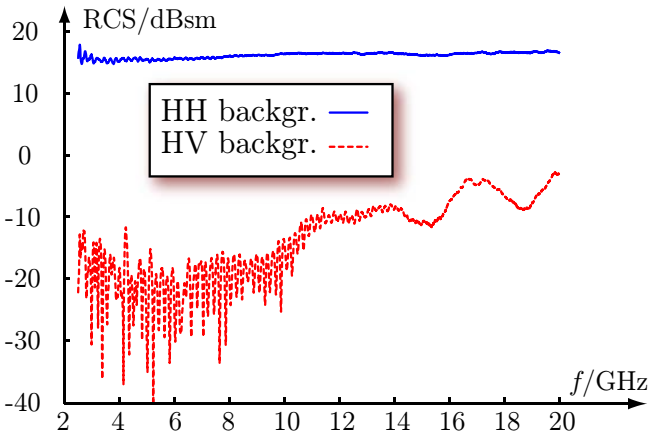

Figure 5. The figure shows the measured calibrated backgrounds for HH and HV polarizations before background subtraction.

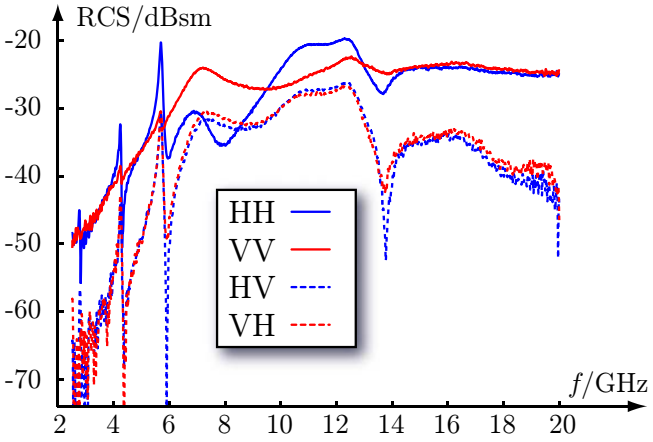

Figure 6. The figure shows the measured linearly polarized forward RCS components.

5 Conclusions

A method to determine the extinction cross section utilizing forward RCS measurements is developed. It can be used to determine the extinction cross section in the frequency range 2.5–38 GHz.

It is found that a calibration using a calibration target is more accurate than an alternative calibration method that does not require a calibration target. It is concluded that the alternative method needs further analysis to be useful for this purpose.

It is suggested that changes in the relative distance from transmitting antenna to receiving antenna are the limiting factor for the background subtraction efficiency. It is found that the combined effect of coherent background subtraction and time domain gating is to suppress the background by 75 dB at low frequencies and by 50 dB at high frequencies. This results in a remaining background level of –60 dBsm at low frequencies and –35 dBsm at high frequencies for a forward RCS measurement.

The method is validated by measuring small metal spheres with known extinction cross sections. It is determined that the extinction cross section can be measured with good accuracy down to a level of –30 dBsm for the investigated frequency range. Measurements of the RCS amplitude linear

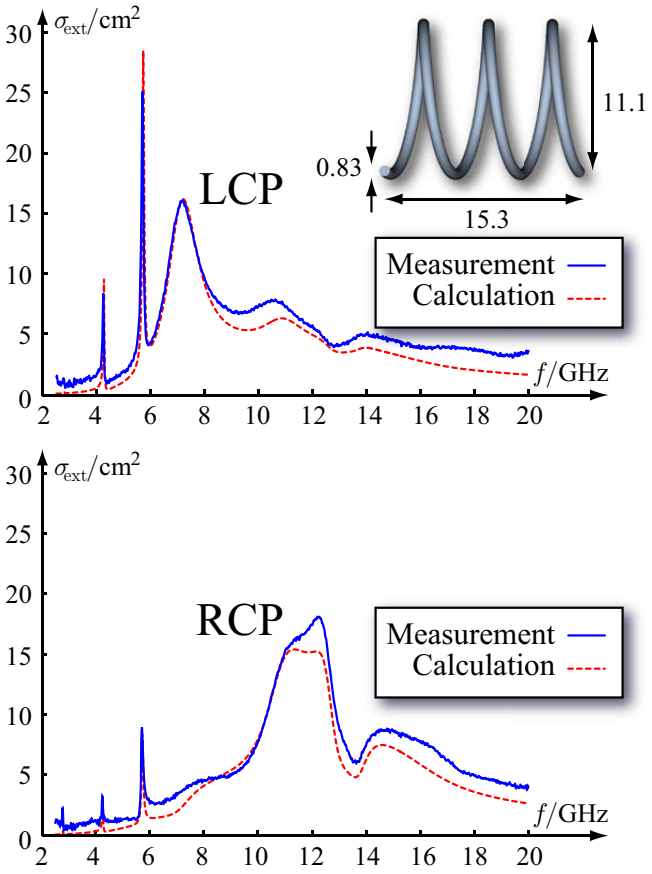

Figure 7. The figure shows the extinction cross sections, $\sigma_{\text{ext}}(f)$, for left circular (LCP)(top) and right circular (RCP)(bottom) polarization of the incident wave determined from experiments and calculations. A drawing of the helix (dimensions in mm) used in the experiments is shown as an insert.

polarization components can be used to calculate the extinction cross section for a circular polarized incident wave.

Acknowledgements

The financial support by the Swedish Foundation for Strategic Research and the Swedish Defense Materiel Administration is gratefully acknowledged.

6 References

[1] C. Sohl, M. Gustafsson, and G. Kristensson, "Physical limitations on broadband scattering by heterogeneous obstacles," *J. Phys. A: Math. Theor.*, vol. 40, pp. 11 165–11 182, 2007.

[2] M. Gustafsson, C. Sohl, and G. Kristensson, "Illustrations of new physical bounds on linearly polarized antennas," *IEEE Trans. Antennas Propagat.*, vol. 57, no. 5, pp. 1319–1327, May 2009.

[3] C. Larsson, M. Gustafsson, and G. Kristensson, "Wideband microwave measurements of the extinction cross section — experimental techniques," Lund University, Department of Electrical and Information Technology, P.O. Box 118, S-221 00 Lund, Sweden, Tech. Rep. LUTEDX/(TEAT-7182)/1–22/(2009), 2009, `http://www.eit.lth.se`.

[4] E. F. Knott, J. F. Shaeffer, and M. T. Tuley, *Radar Cross Section*. 5601 N. Hawthorne Way, Raleigh, NC 27613: SciTech Publishing Inc., 2004.

[5] G. T. Ruck, D. E. Barrick, W. D. Stuart, and C. K. Krichbaum, *Radar Cross-Section Handbook*. New York: Plenum Press, 1970, vol. 1 and 2.

[6] R. Newton, "Optical theorem and beyond," *Am. J. Phys*, vol. 44, pp. 639–642, 1976.

[7] M. I. Skolnik, *Introduction to radar systems*, 3rd ed. Boston: McGraw-Hill, 2001.

[8] E. Zdansky, A. Örbom, and J. Rahm, "Object-free calibration and procedures for bistatic wideangle ISAR measurements of clutter reflectivity at the Lilla Gåra (Sweden) test range," in *Proc. Antenna Measurement Techniques Association (AMTA)*, Atlanta, Georgia, 2010, pp. 1–6.

[9] D. R. Lide, *CRC handbook of chemistry and physics : a ready-reference book of chemical and physical data. Ed. 88 (2007-2008)*. Boca Raton, Florida: CRC Press, 2008.

[10] B. M. Welsh, B. M. Kent, and A. L. Buterbaugh, "Full polarimetric calibration for radar cross-section measurements: Performance analysis," *IEEE Trans. Antennas Propagat.*, vol. 52, no. 9, pp. 2357–2365, 2004.